

MICROMACHINED STIMULATING ELECTRODES

Quarterly Report #3

(Contract NIH-NINDS-N01-NS-5-2335)

April 1996 --- June 1996

RECEIVED CMB/NINDS

96 JUL 26 A9 53

Submitted to the

Neural Prosthesis Program

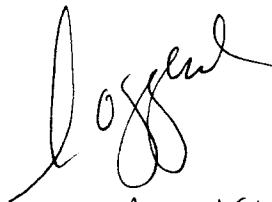
National Institute of Neurological Disorders and Stroke
National Institutes of Health

by the

Center for Integrated Sensors and Circuits

Department of Electrical Engineering and Computer Science
University of Michigan
Ann Arbor, Michigan
48109-2122

July 1996


7/24/96

MICROMACHINED STIMULATING ELECTRODES

Summary

During the past quarter, work in this program has gone forward in several areas. We have continued to fabricate passive probe structures for internal and external users. Working in conjunction with the Center for Neural Communication Technology, additional probes from one mask set have been realized, a new mask set containing probe designs from five external users has been designed, and probes from this new mask set are now in fabrication. We have also performed detailed characterization studies on chronically-implanted iridium oxide stimulating sites in-vivo. Electrochemical impedance spectroscopy (EIS) and cyclic voltammetry (CV) were used to evaluate chronically stimulated sites in six animal experiments in guinea pig cortex using 21 separate sites. The probes consisted of sites varying from $400\mu\text{m}^2$ to $1600\mu\text{m}^2$ in size. Stimulation began after a 10-17 day recovery period. Biphasic current pulses (variable magnitude, $100\mu\text{sec/phase}$, 250pps) were applied both bipolarly and monopolarly for two hours on five consecutive days. These current pulses reduced the charge storage and increased the site impedances at low frequencies, implying a change in the iridium oxide. The low-frequency change is permanent, in that a night of rest did not return the impedance spectrum to its pre-stimulation levels. Current pulsing also affects the impedance spectrum at mid-range frequencies, with the magnitude decreasing after stimulation. However, this decrease appears to be temporary, with magnitude returning to a higher value by the next day. The impedance change effected by current pulses takes place after a relatively few number of pulses have been applied. Additionally, some data suggests that a significant effect is seen in the electrical characteristics as a result of implantation. During the coming quarter, the data will be examined more analytically and the effects of encapsulation and healing will be examined more thoroughly. Histological results should also be available then for these experiments.

Two key areas in the further development of active stimulating probes involve the development of low-resistance interconnect materials and improvements in making circuit contacts. Both of these areas were undertaken during the past term. Both tantalum and titanium silicide interconnects were formed using co-sputtering and found to exhibit sheet resistances of about 3.5 ohms per square. This is three to four times better than the highly doped polysilicon currently used on the probes. We plan further experiments using refractory salicides, refractory metal cores, and optimization of the present co-sputtering approach to try to reduce the resistance another factor of three. In the area of circuit contacts, five different approaches to contact formation were explored in connection with the basic reactive ion etching process. Of these, the use of a modest RIE overetch followed by either an NOE descum cleaning step or an oxygen plasma cleaning step produced the best results. The contacts were greatly improved over other approaches, at least before sintering; after sintering all of the approaches appeared to produce similar results. Additional experiments to try to lower the contact resistances further are planned along with experiments using PtSi and TiN or TiW plugs in the contacts. Processing will then go forward to completion on a new set of active stimulating probes. The design of a new 64-site four-channel stimulating probe with off-chip current generation is also nearing completion.

MICROMACHINED STIMULATING ELECTRODES

1. Introduction

The goal of this research is the development of active multichannel arrays of stimulating electrodes suitable for studies of neural information processing at the cellular level and for a variety of closed-loop neural prostheses. The probes should be able to enter neural tissue with minimal disturbance to the neural networks there and deliver highly-controlled (spatially and temporally) charge waveforms to the tissue on a chronic basis. The probes consist of several thin-film conductors supported on a micromachined silicon substrate and insulated from it and from the surrounding electrolyte by silicon dioxide and silicon nitride dielectric films. The stimulating sites are activated iridium, defined photolithographically using a lift-off process. Passive probes having a variety of site sizes and shank configurations have been fabricated successfully and distributed to a number of research organizations nationally for evaluation in many different research preparations. For chronic use, the biggest problem associated with these passive probes concerns their leads, which must interface the probe to the outside world. Even using silicon-substrate ribbon cables, the number of allowable interconnects is necessarily limited, and yet a great many stimulating sites are ultimately desirable in order to achieve high spatial localization of the stimulus currents.

The integration of signal processing electronics on the rear of the probe substrate (creating an "active" probe) allows the use of serial digital input data which can be demultiplexed on the probe to provide access to a large number of stimulating sites. Our goal in this area has been to develop a family of active probes capable of chronic implantation in tissue. For such probes, the digital input data must be translated on the probe into per-channel current amplitudes which are then applied to the tissue through the sites. Such probes require five external leads, virtually independent of the number of sites used. As discussed in our previous reports, we are now developing a series of active probes containing CMOS signal processing electronics. Two of these probes are slightly redesigned versions of an earlier first-generation set of designs and are designated as STIM-1a and STIM-1b. A third probe, STIM-2, is a second-generation version of our high-end first-generation design, STIM-1. All three probes provide 8-bit resolution in setting the per-channel current amplitudes. STIM-1A and -1B offer a biphasic range using $\pm 5V$ supplies from $0\mu A$ to $\pm 254\mu A$ with a resolution of $2\mu A$, while STIM-2 has a range from 0 to $\pm 127\mu A$ with a resolution of $1\mu A$. STIM-2 offers the ability to select 8 of 64 electrode sites and to drive these sites independently and in parallel, while -1a allows only 2 of 16 sites to be active at a time (bipolar operation). STIM-1b is a monopolar probe, which allows the user to guide an externally-provided current to any one of 16 sites as selected by the digital input address. The high-end STIM-2 contains provisions for numerous safety checks and for features such as remote impedance testing in addition to its normal operating modes. It also offers the option of being able to record from any one of the selected sites in addition to stimulation.

During the past quarter, we have continued to fabricate passive probe structures for internal and external users. Working in conjunction with the Center for Neural Communication Technology at the University of Michigan, additional probes from one mask set have been realized, a new mask set has been designed, and probes from this new mask set are now in fabrication. We have also performed detailed characterization studies of chronically-implanted stimulating sites and have begun technology studies aimed at the

development of low-resistance interconnect materials and low-resistance circuit contacts for the active stimulating probes. The results in each of these areas are described below.

2. *In-Vivo Iridium Oxide Characterization Studies*

In order to develop electrode arrays capable of stimulating neural structures on a chronic basis, it is necessary to understand and then optimize the interface between the iridium oxide stimulating sites and the tissue. Electrochemical impedance spectroscopy (EIS) and cyclic voltammetry (CV) were used to evaluate chronically stimulated electrodes during the past quarter. Six animal experiments have been completed, with 21 separate electrode sites evaluated.

Chronic Stimulation Experiments

A chronic stimulating probe was implanted in the cortex of a guinea pig using methods previously described. The probe consisted of 6 or 8 sites of varying size ($400\mu\text{m}^2$ to $1600\mu\text{m}^2$). Stimulation began after a 10-17 day recovery period. Biphasic current pulses (variable magnitude, $100\mu\text{sec/phase}$, 250 pulses/sec) were applied both bipolarly and monopolarly for two hours on five consecutive days. (Previous experiments stimulated for four hours, but results from those experiments showed that impedance changes usually occur in the first few minutes of pulsing. The stimulation time was shortened to two hours so that more sites could be tested in one day. Two hours is a sufficient amount of time to produce a change in the impedance and still accumulate a significant number of pulses, 1.8 million per day.) EIS and CV data were collected on each stimulated site and one unstimulated control site during the week, before and after the two hours of stimulation. The measurement system included a potentiostat (EG&G 283), a frequency response analyzer (EG&G 1025), and a 486 PC. The test cell consisted of the activated iridium stimulation site (working) and two 316 stainless steel head screws (counter and reference).

Cyclic voltammograms were collected at scan rates of 100, 250, 500, and 1000mV/sec . The voltage limits were -0.6V to 0.9V vs. 316SS. The only consistent result presently apparent is that the CV curve will change shape after one day of stimulation and then maintain this new shape throughout the week. The curves below (Fig. 1) were taken from a $1200\mu\text{m}^2$ site (scan rate 250mV/sec). The top curve shows a CV taken two weeks post implant, before any stimulation (thin line) and after the first day of stimulation (thick line). The charge storage capacity (Q_{cap}) decreases as a result of stimulation, from $0.2\mu\text{C}$ to $0.09\mu\text{C}$ (as measured by integrating under the entire area of the CV curve). CV curves from before and after stimulation on the second day (Fig. 1 bottom) show that the Q_{cap} does not change significantly after the first day. Figure 2 shows charge storage values for this site for an entire week of stimulation. After the initial decline on the first day, Q_{cap} remains fairly constant for the remainder of the week. Current pulses of $50\mu\text{A}$ for $100\mu\text{sec}$ were used on this site, resulting in a total of 5nC delivered to the site every pulse. A safe (within the water window) measure for injectable charge with a current pulse has been estimated to be approximately 10% of Q_{cap} ¹. In this case, the lowest value for Q_{cap} is 63nC , which allows 6.3nC to be safely injected. Therefore, 5nC appears to be a safe charge/phase.

¹Robblee, L.S., et. al., "Studies of the Electrochemistry of Stimulating Electrodes", Final Report, NIH Contract No. N01-NS-8-2313, August 1991.

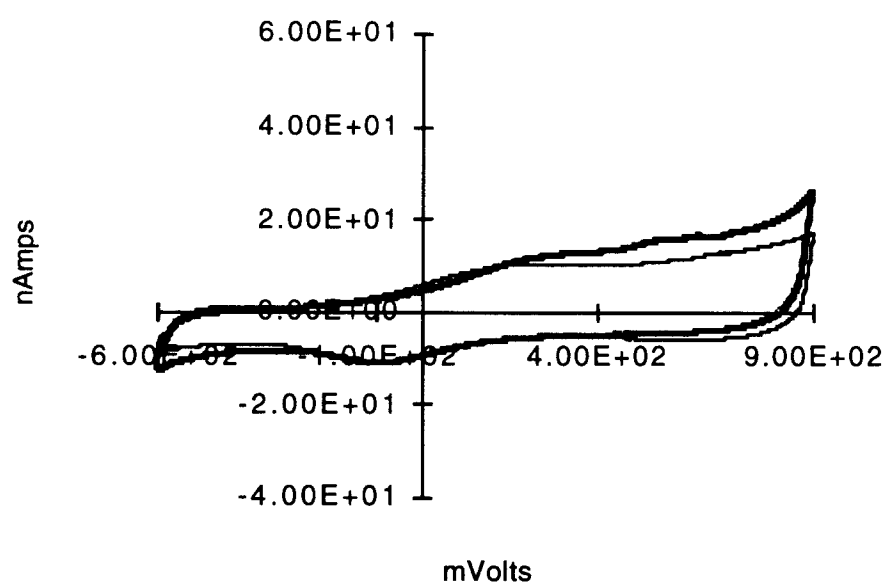
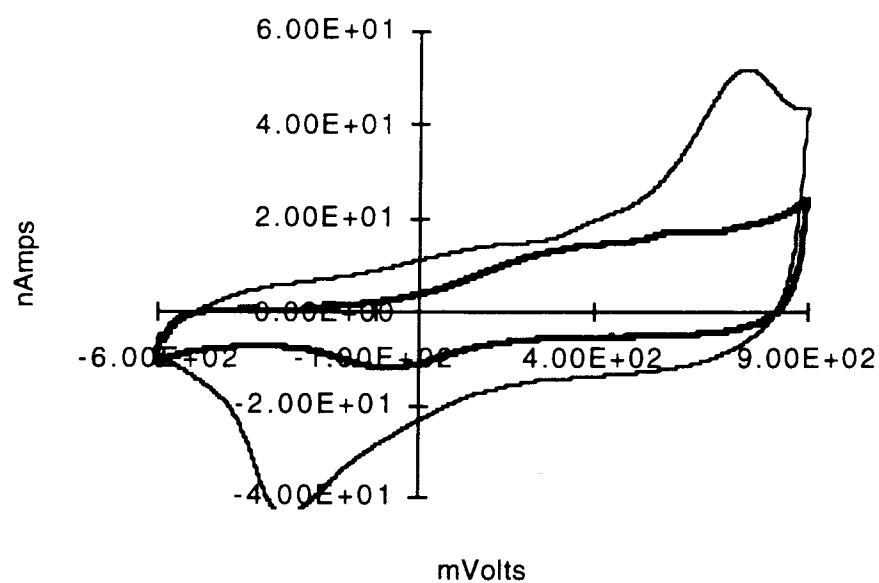


Fig. 1: *In vivo* CV curves of a $1200\mu\text{m}^2$ site before day 1 stimulation (top thin), after day 1 stimulation (top thick), before day 2 stimulation (bottom thin), and after day 2 stimulation (bottom thick).

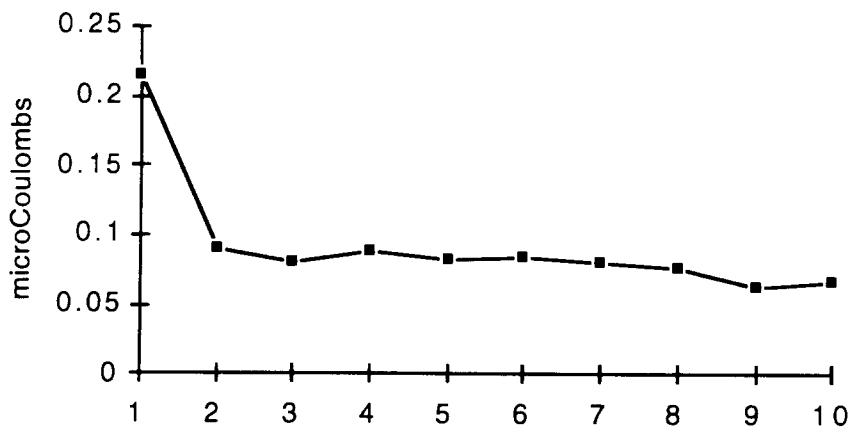


Fig. 2: Charge storage measurements for one week of stimulation for a $1200\mu\text{m}^2$ site (1-before day 1, 2-after day 1, etc.).

The impedance data corresponding to the above CV curves is shown below (Figs. 3, 4). The general trend for the impedance spectra before and after stimulation is summarized below for three frequency regions.

- Low frequency impedance (below 100Hz) increases after the first day of stimulation and remains at the increased level.
- Mid-range impedance (100Hz-100kHz) decreases temporarily after stimulation but returns to pre stimulation levels overnight.
- High frequency impedance (over 100kHz) changes little.

The low frequency impedance increase after stimulation correlates with the change in the CV curves shown above. The ramp wave used for CV testing is a slow wave (i.e., its sinewave components are low frequency). Lower charge storage indicated in a CV curve matches a higher impedance at low frequencies. The impedance increase is maintained after an overnight rest. This too matches the CV data, which shows a permanent change in CV shape. These data support the model (Robblee [1], discussed below) which attributes the low frequency impedance to the iridium oxide. The mid-range frequency decrease is harder to explain with the present data. This impedance is thought to be related to the efficacy of the charge transfer, which depends on oxide morphology, proton concentration, and the impedance of the current flow path through tissue. Methods are being sought which will reveal tissue changes which relate to the *in vivo* component of the impedance. The high frequency impedance is due to the series resistance, double layer capacitance, and cell capacitance (shunt current from silicon cable, test leads, and so forth).

Neither the decreased charge storage nor the impedance reduction at mid-range frequencies appear to have a significant impact on the back voltage developed at the electrode (Fig. 5). The current pulse is a fairly high frequency signal, so it follows from the impedance spectrum that any changes in the low frequency response characteristics would have little effect on back voltage. The pulse on the left was taken at the beginning of the first day while the pulse on the right was taken at the end of the last day. There is a

slight drop in the voltage level, but the difference is not on the order of the impedance change seen at mid-range frequencies.

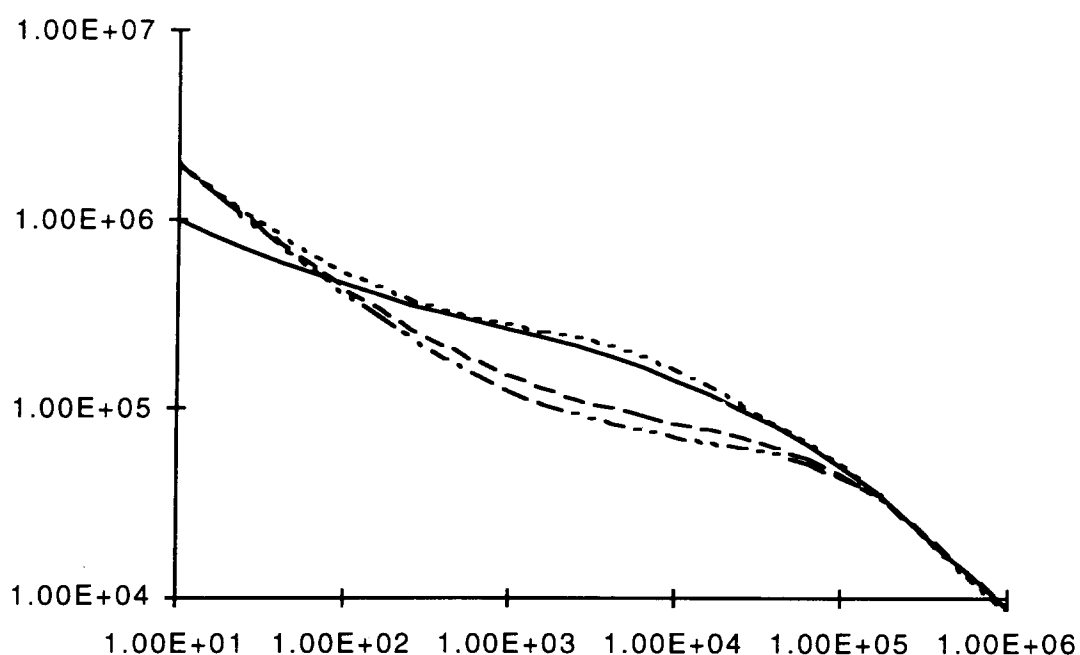


Fig. 3: *In vivo* impedance magnitude before day 1 stimulation (solid), after day 1 stimulation (dashed), before day 2 stimulation (dotted), and after day 2 stimulation (dash-dot).

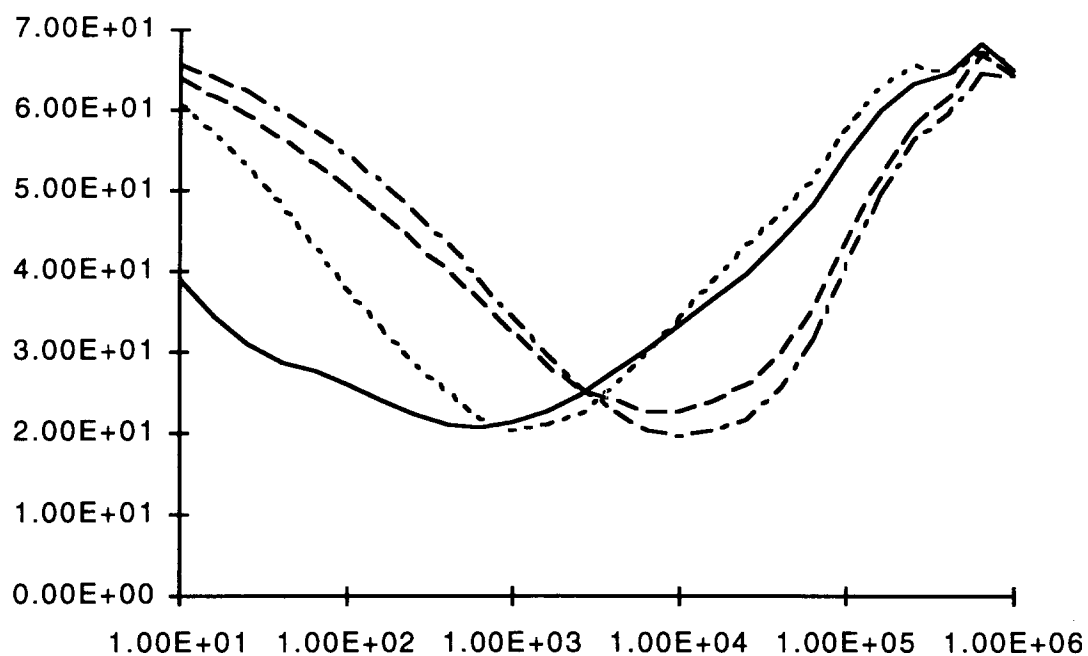


Fig. 4: *In vivo* impedance phase before day 1 stimulation (solid), after day 1 stimulation (dashed), before day 2 stimulation (dotted), and after day 2 stimulation (dash-dot).

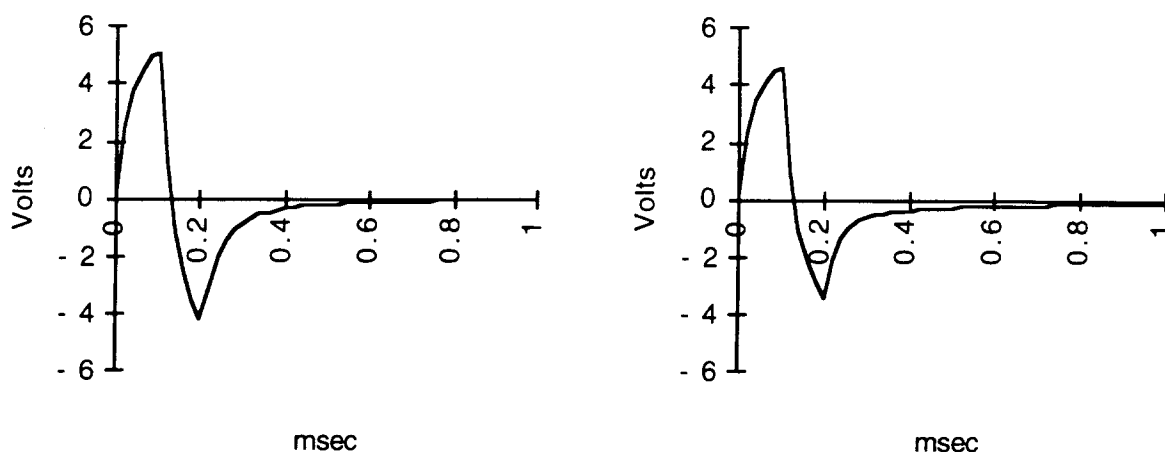


Fig. 5: Back voltage at $1200\mu\text{m}^2$ electrode in response to a $50\mu\text{A}$ pulse at the beginning of the first day of pulsing (left) and at end of fifth day of pulsing (right).

The waveforms in Fig. 5 are averages of 100 pulses. An experiment was run to determine when current pulsing affected the back voltage and impedance. A train of 100 pulses was recorded without averaging. Figure 6 plots the back voltage from the first pulse, the 100th pulse, and after two minutes of pulsing. Within the first 100 pulses the back voltage declines noticeably. After only two minutes the decrease is even more significant. Additionally, IS data were taken before and after the two minutes of pulsing (Figs. 7, 8). Clearly, even a short time of pulsing results in a significant shift in the impedance spectrum. The data below was the only instance examined. More extensive testing of the time course of the impedance change will be undertaken next quarter.

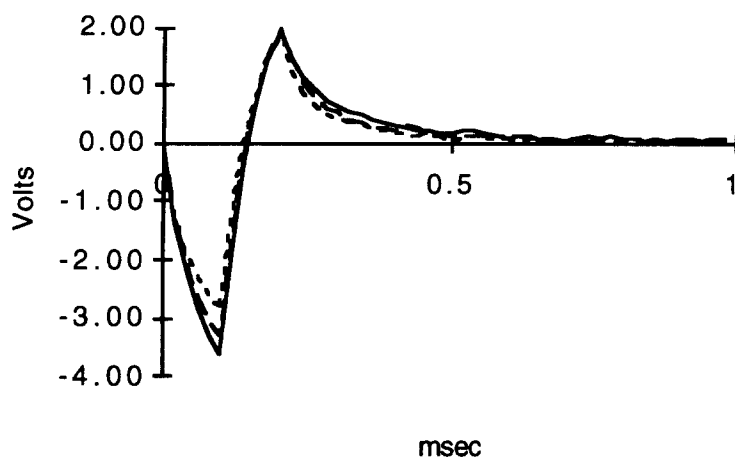


Fig. 6: Back voltage at a $800\mu\text{m}^2$ site in response to a $25\mu\text{A}$ pulse for the first pulse (solid), the 100th pulse (dashed), and the pulse after 2 minutes (dotted).

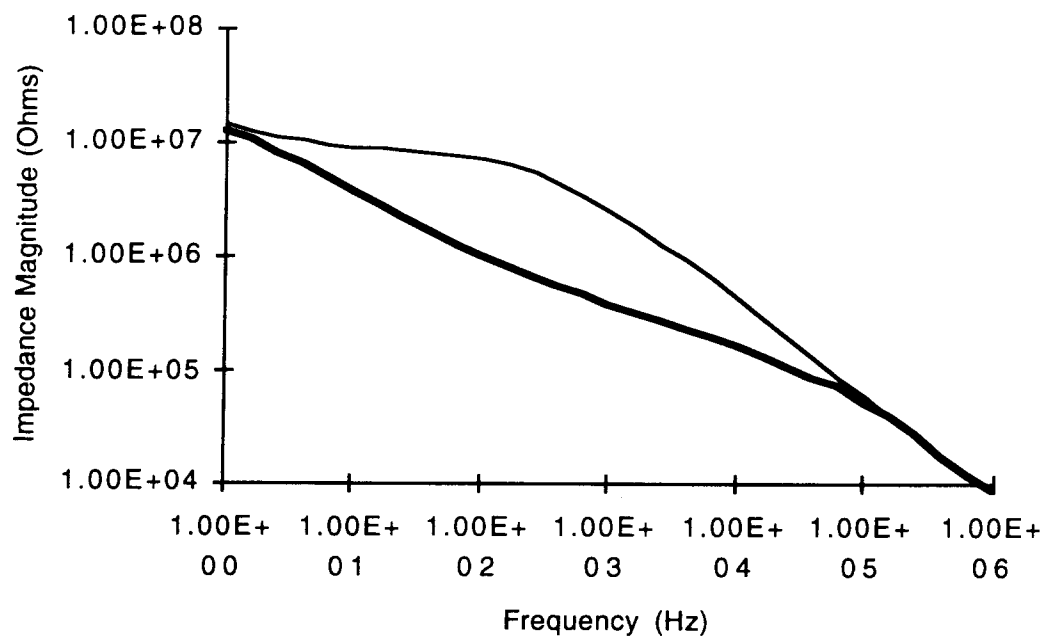


Fig. 7: Impedance magnitude of a $800\mu\text{m}^2$ site before (thin) and after (thick) two minutes of current pulsing ($25\mu\text{A}$, $100\mu\text{sec}/\text{phase}$, 250 pps).

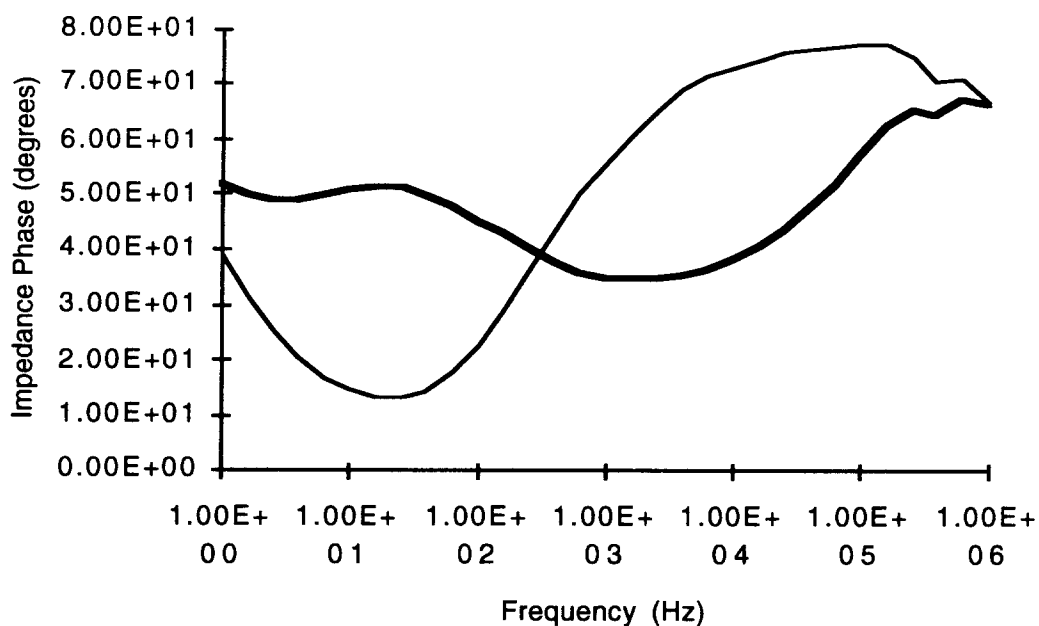


Fig. 8: Impedance phase of a $800\mu\text{m}^2$ site before (thin) and after (thick) two minutes of current pulsing ($25\mu\text{A}$, $100\mu\text{sec}/\text{phase}$, 250 pps).

In summary, applying current pulses reduces the charge storage and increases the impedance at low frequencies, implying a change in the iridium oxide. The low frequency

change is permanent, in that a night of rest does not return the impedance spectrum to its pre-stimulation levels. Current pulsing also affects the impedance spectrum at mid-range frequencies, with the magnitude decreasing after stimulation. However, this decrease appears to be temporary, with magnitude returning to a higher value by the next day. It should also be noted that although the experiment discussed above typified the data collected this quarter, there were some exceptions and variability, particularly in the response (as measured by CV) of the iridium oxide to stimulation. The experimental conditions for these tests exceptions will be examined and any findings will be mentioned in future reports.

Other observations

We continue to see indications that the electrical characteristics of the sites change during the healing/encapsulation process, and that these changes can be improved (i.e., the impedance can be lowered) by "conditioning" the site. Figure 9 below shows CV data taken two weeks post-op. The animal was not stimulated or tested during that recovery period. The three curves were taken consecutively (250mV/sec), before the first day of stimulation. Comparing the shape of the first curve to the second and third, the current peaks of the second and third curves are slightly closer together, indicating that the redox reactions proceeded more readily in the later CVs.

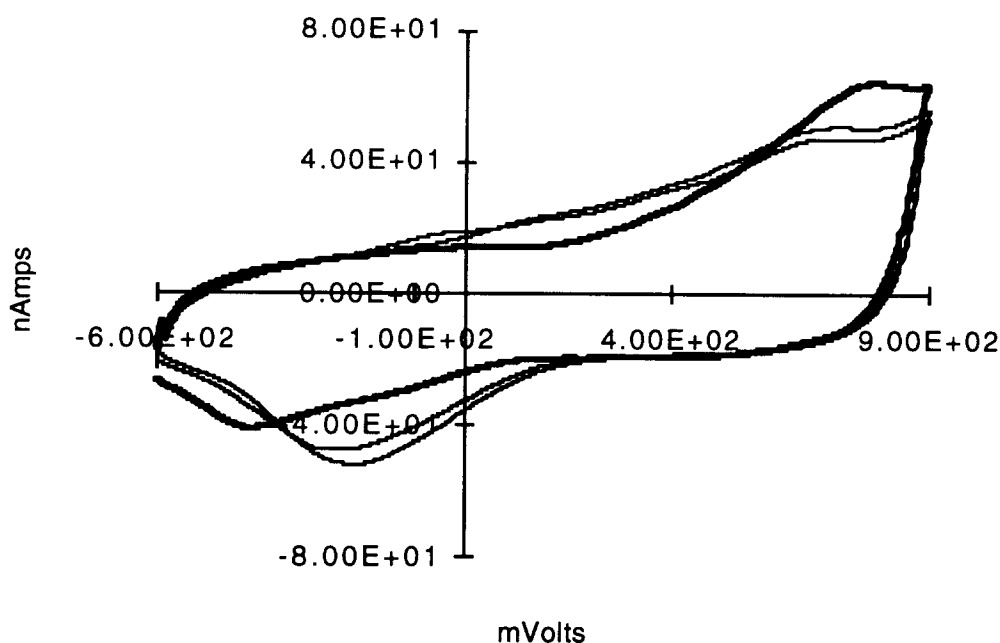


Fig. 9: Three consecutive CVs on a 1600 μm^2 site, two weeks after implant: first CV (thick line), second and third CVs (thin lines).

The CV tests themselves appear to change the electrode-tissue system in some way. Figures 10-11 show the impedance spectra of a site taken before the site was stimulated. The dashed line was measured before CV testing, the solid line after.

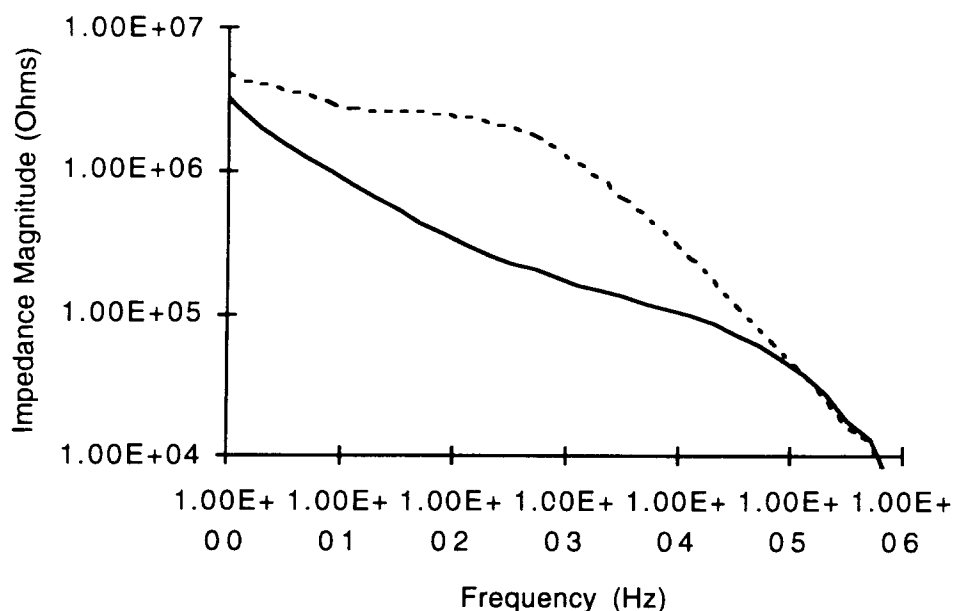


Fig. 10: Impedance magnitude of a $1600\mu\text{m}^2$ site before (dashed) and after CV testing.

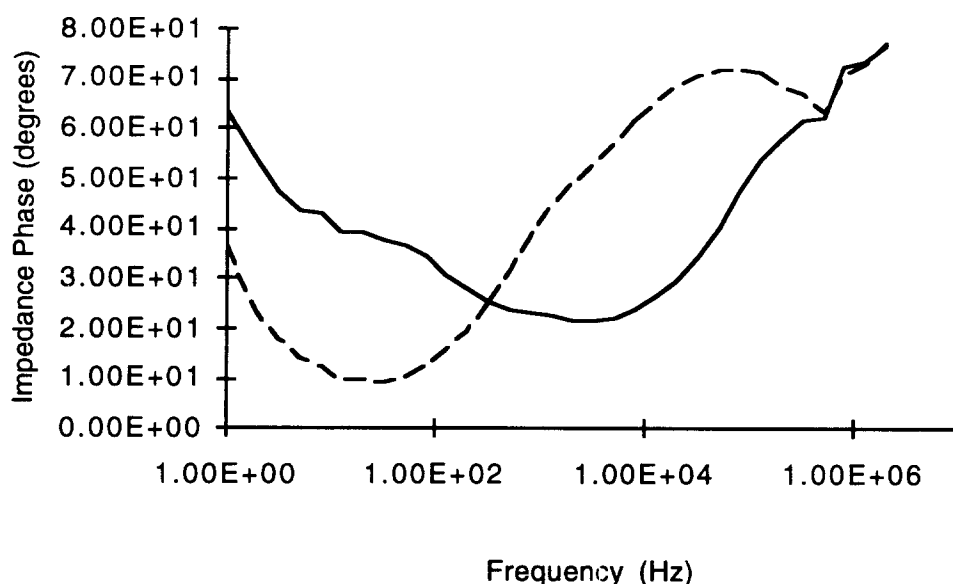


Fig. 11: Impedance phase of a $1600\mu\text{m}^2$ site before (dashed) and after CV testing.

The data presented above show that the electrical characteristics of the electrode-tissue system are modified by current pulsing and by voltage biasing (with the slow ramp waves of the CV). These observations with large activated stimulating electrodes agree with other data from several investigators using smaller recording electrodes (activated and unactivated). A test protocol, similar to that proposed in Quarterly Report #11 for the Contract "Multichannel Multiplexed Intracortical Recording Arrays," will be executed in the next quarter. The test is summarized in the table below.

Tests	Site 1-2	Sites 3-4	Sites 5-6
Post-operative IS and CV	X	X	X
IS every 2 days	X		
IS and CV every 2 days		X	
IS after 2 weeks	X	X	X
IS after 2 weeks, CV testing, and current pulsing	X	X	X

The test is designed to measure the changes in the electrical characteristics of the tissue over the two week rest period allotted to the chronic implant.

Modeling

A circuit model of the interface can be constructed. Impedance data can then be fitted to a particular model and component values assigned to the circuit. The model used was first proposed by investigators at EIC² and is shown schematically in Fig. 12. The validity of this model is currently under discussion, but it will be used in our initial attempt to explain the impedance data. The curve fitting procedure involves making an initial estimate of parameter values based on graphical information from the Nyquist plot and then letting the program minimize the square error by varying the model parameters from the initial estimate. The user can fit a section of the curve or the entire curve. Weighting of points is possible to put emphasis on more reliable data. The program outputs final model parameters, the number of iterations, and the goodness of fit parameter C².

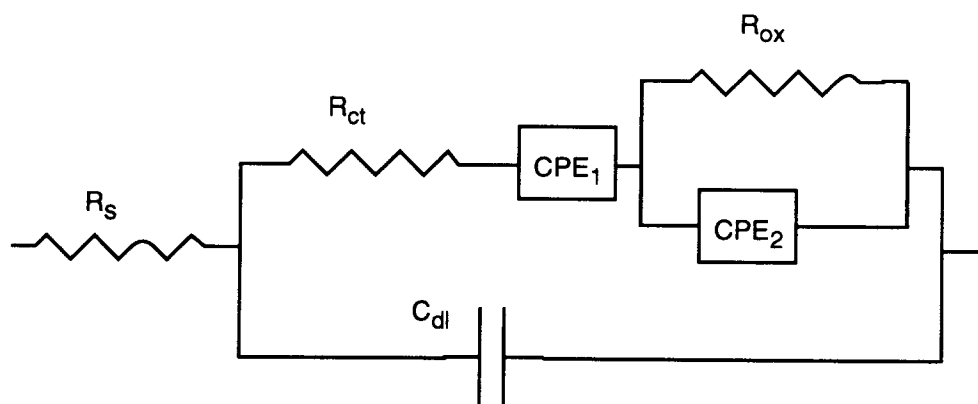


Fig. 12: A circuit model of an iridium oxide stimulating site.

The elements of the model are attributable to physical components of the electrode tissue system. R_s is the series resistance. C_{dl} is the double layer capacitance of the iridium metal. R_{ct} represents the charge transferred from oxide to solution via Faradaic reactions. CPE_1 (Constant Phase Element) acknowledges that the ion flow for charge transfer must travel through pores, resulting in a distributed response. R_{ox} and CPE_2 are the resistance and "capacitance" of the oxide. Again, due to the porous nature of the iridium, the

²Aurian-Blajeni, B. et al. "Impedance of Hydrated Iridium Oxide Electrodes", *Electrochimica Acta*, Vol. 34, No. 6, pp. 795-802, 1989.

capacitance of ions in the pores to the oxide will be distributed with the resistance to ion flow in the pores. Modeling of the EIS data will be attempted next quarter.

Conclusion

The effort this past quarter has been focused on data acquisition and making general observations on the effect of current pulsing and low frequency potential cycling. The iridium oxide film was affected by the pulses, reflected in an increase in low frequency impedance and a decrease in charge storage. This change was permanent. Impedance in the mid-range was decreased after stimulation. This decrease was temporary, however, with the impedance returning to its higher level overnight. The impedance change effected by current pulses takes place after a relatively few number of pulses have been applied. Additionally, some data was taken that suggests a significant effect is seen in electrical characteristics as a result of implantation. In the next quarter, the data will be examined more analytically, using modeling as described above. Also, the effect of encapsulation and healing will be examined more thoroughly. Histological results will be available for the experiments reported here.

3. Active Stimulating Probe Development

In the development of active probes, we are in the process of fabricating more of the first- and second-generation probe designs, of iterating the design on our high-end second-generation stimulating probe (STIM-2), and of designing a simplified stimulating probe having four input current channels and four on-chip 16:1 site selectors capable of steering these currents to appropriate sites. As part of these efforts, the development of low-resistance interconnects to replace our current polysilicon material and the development of improved contact processes for circuit fabrication are both essential. These two areas were the focus for considerable work during the past quarter as described below.

Development of Low-Resistance Interconnect Materials

We are currently working on the development of methods for the in-house fabrication of a low-resistance interconnect material for use on the active and passive probes. Two silicides, TaSi_2 and TiSi_2 , are being considered, as well as several different techniques for forming these silicides. Low-resistance interconnect will play an important role in the fabrication of neural probes by reducing the voltage drop along the interconnect lines, an option that is especially important for long ribbon cable designs.

Silicide is formed through the combined deposition of a refractory metal and silicon, followed by a high temperature anneal in an inert ambient. During the anneal, the refractory metal reacts with silicon wherever the two are in contact to form a silicide. The use of silicide as an interconnect material is advantageous because its sheet resistance is approximately one order of magnitude lower than that of polysilicon. Although this is still up to an order of magnitude higher than the sheet resistance of solid aluminum or refractory metals, silicide adheres to the surrounding dielectrics much better than the pure metals do and is able to withstand subsequent processing temperatures several hundred degrees higher than can be withstood by many solid metals.

The two methods we are looking at for fabricating the silicides are a co-sputtering approach and a 'wrap' technique. In the co-sputtering method, a refractory metal and silicon are sputtered simultaneously onto the wafer, then lifted off or etched to obtain the

desired pattern. The sputtering is followed by a high temperature anneal, allowing the two materials to react and form a silicide. In the wrap method, polysilicon is first deposited and patterned, and a refractory metal then sputtered or evaporated on top of the poly. When the wafer is subsequently annealed, the metal reacts to form a silicide only where there is polysilicon beneath it. The unreacted metal is removed in a selective wet etch, leaving behind silicide over the patterned poly. We use the term 'wrap' because the resulting interconnect consists of a polysilicon core wrapped in silicide. This material is also known as salicide, for 'self-aligned silicide', because no separate alignment and patterning of the silicide is necessary, as it automatically forms in the pattern of the poly core.

We are first investigating the co-sputtering method for silicide formation. We have characterized the sputter deposition rates of tantalum, titanium, and silicon at different sputtering powers and used this information to determine the relative powers needed to sputter the desired atomic ratio of metal and silicon. Post-sputtering anneals at several different temperatures have revealed the effect of temperature on resulting silicide sheet resistance. A temperature of at least 600°C is necessary for the silicide-forming reaction to occur, and a 30 minute anneal at 700°C produces a sheet resistance of approximately 3.5 ohms per square. We are currently experimenting with different annealing times and temperatures to optimize these parameters and lower the sheet resistance to approximately 1 ohm per square. We will also experiment with lower sputtering pressures and higher metal-to-silicon atomic ratios to help lower the resistance.

After optimizing co-sputtered silicide formation, we will investigate wrap techniques and compare the characteristics of the resulting interconnect, as well as the ease and practicality of fabrication, of the two methods. We have designed and fabricated a mask set which contains structures to test the characteristics of different interconnects. The test structures include devices to test sheet resistance, step coverage and adhesion to dielectrics.

Circuit Contacts

In the past, circuit contacts have caused significant problems in realizing working and reliable circuits on all of our active probes. This has been attributed to various causes, including polymer formation, low substrate surface doping density (contact not ohmic), surface damage, and so forth; all of these are associated with the dry etching method being used (reactive ion etching (RIE)). Attempts have previously been made to circumvent the problem by using an O₂ plasma etch in the RIE after the normal oxide etch, buffered HF dips prior to metal deposition, or annealing steps after contact formation. These have, in general, all met with some degree of success, but not with the reliability that is necessary to achieve yields as high as are desirable in the circuit areas. Based on an extensive literature study, we have compared the following methods (all of which use RIE as the basic etch method) for forming low-resistance contacts:

- 1) RIE only
- 2) RIE followed by a buffered hydrofluoric acid (BHF) dip
- 3) RIE followed by a wet descum agent, NOE
- 4) RIE followed by a wet descum agent, EKC 265
- 5) RIE followed by a 400°C O₂ anneal and subsequent BHF dip

As a control, contacts were also formed by wet etching with BHF. This method is assumed to leave no residue in the contact opening; therefore, it should form the best contact. Unfortunately, this method is not useful in actual circuit contacts because the

isotropic nature of the etch results in large lateral etching of the contacts under the masking photoresist, which can lead to the possibility of circuit shorts.

The general process for the wafers used in the contact tests was:

- 1) grow an oxide
- 2) deposit polysilicon
- 3) dope the polysilicon with phosphorus
- 4) pattern the polysilicon
- 5) grow a pad oxide
- 6) deposit LPCVD oxide
- 7) pattern for the contact etch
- 8) RIE (or wet etch) the contacts
 - a) half of the RIE wafers with a 10-25% over-etch
 - b) half of the RIE wafers with a >50% over-etch
- 9) perform the various post-RIE treatment methods to different wafers
- 10) pattern for metal
- 11) sputter metal, Al/Si (1/2%)
- 12) perform lift-off
- 13) measure contact resistance with Kelvin bridge structures (pre-sinter contact resistance)
- 14) anneal in a N_2/H_2 forming gas
- 15) measure contact resistance with Kelvin bridge structures (post-sinter contact resistance)

All of the wafers were processed the same in steps 1-7, 10-15. Steps 8 and 9 were essentially the only points where the wafers were processed differently.

The contact resistances of the various treatment methods was measured using an HP4145 circuit analyzer to force a current sweep over the range of 0-100 μ A while monitoring the voltage drop developed across the contact with high input impedance channels. The slope of the voltage drop versus current relationship is then used to find the resistance of the contact. Figures 13-16 demonstrate the I-V characteristics of some of the pre-sinter contacts. A calculated resistance is also plotted on the same graph. Figures 13-14 show typical plots of the I-V characteristics of the RIE only with 10% over-etch and RIE (50% over-etch) + EKC 265, respectively. These have very high resistance and are non-linear. The RIE only plot is very similar to the BHF dipped contacts. Figures 15-16 show plots of RIE (50% over-etched) + NOE cleaned and RIE (50% over-etched) + O_2 annealed I-V characteristics. These have relatively low resistances and linear characteristics even at the over-etch level. A summary of all of the pre-sinter contact resistances is shown bar graph in Fig. 17. Each bar is the average of 5 measurements. The bar graph suggests that the EKC265 descum agent is a very poor method, as its resistance dwarfs that of the other methods. In order to see the relative sizes of the other methods, the bar graph of Fig. 18 does not include the EKC 265 method. The RIE + NOE and O_2 anneal methods appear to come the closest to mirroring the performance of the BHF wet etch method.

Sintering the wafers in the N_2/H_2 forming gas greatly improved the contact resistance of all of the methods. Figures 19-23 show that all of the various methods have relatively low resistances and good linearity. Note that the O_2 annealing results are not yet complete. The most dramatic change is seen in the EKC 265 method. It would appear from this data that the method used for contact cleaning is not critically important so long as a sintering step is carried out in N_2/H_2 .

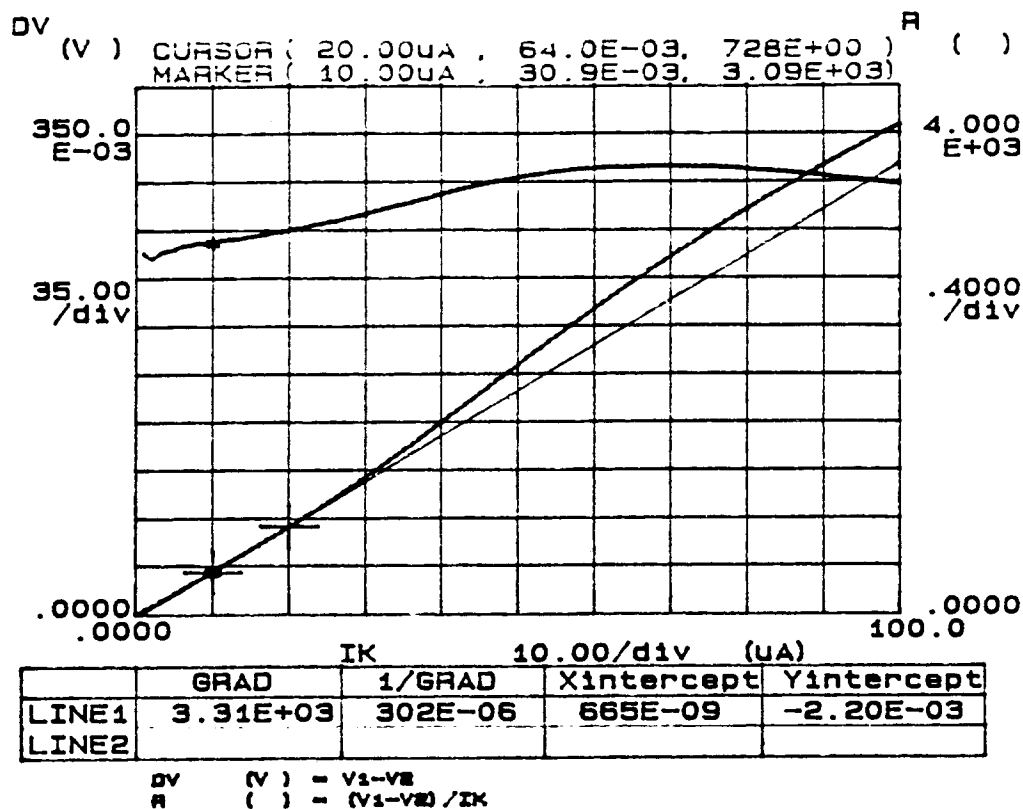


Fig. 13: I-V and resistance plot of a 10% over-etched RIE-only contact.

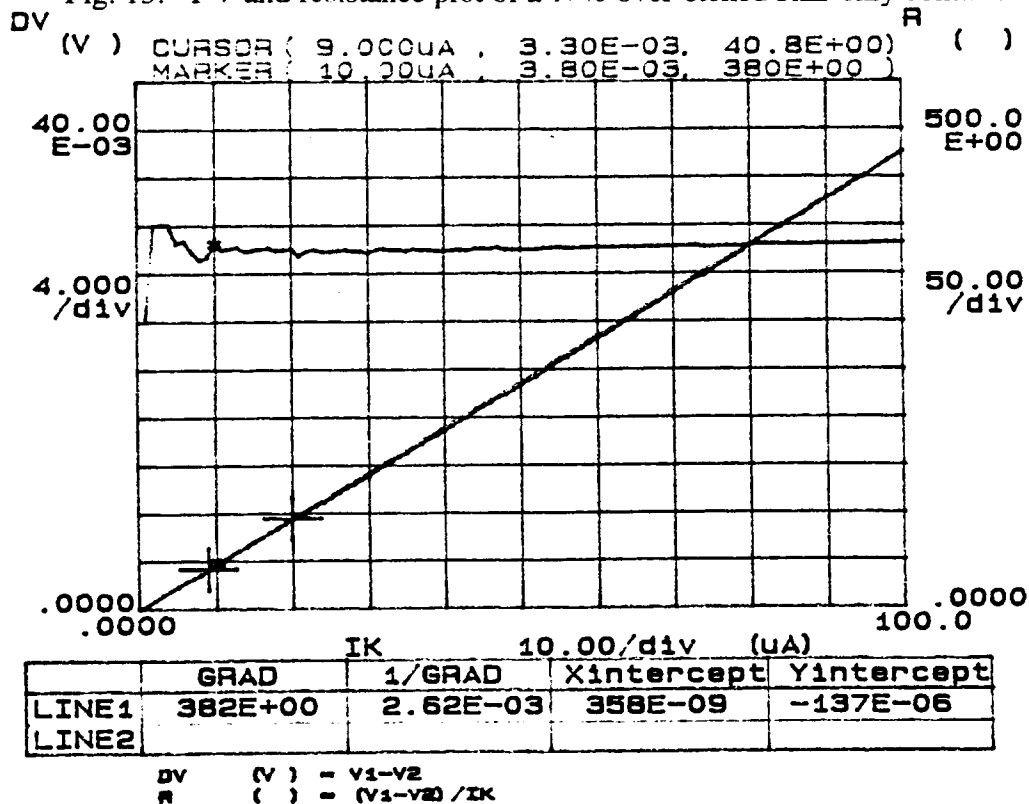


Fig. 14: I-V and resistance plot of a 50% over-etched RIE + NOE cleaned contact.

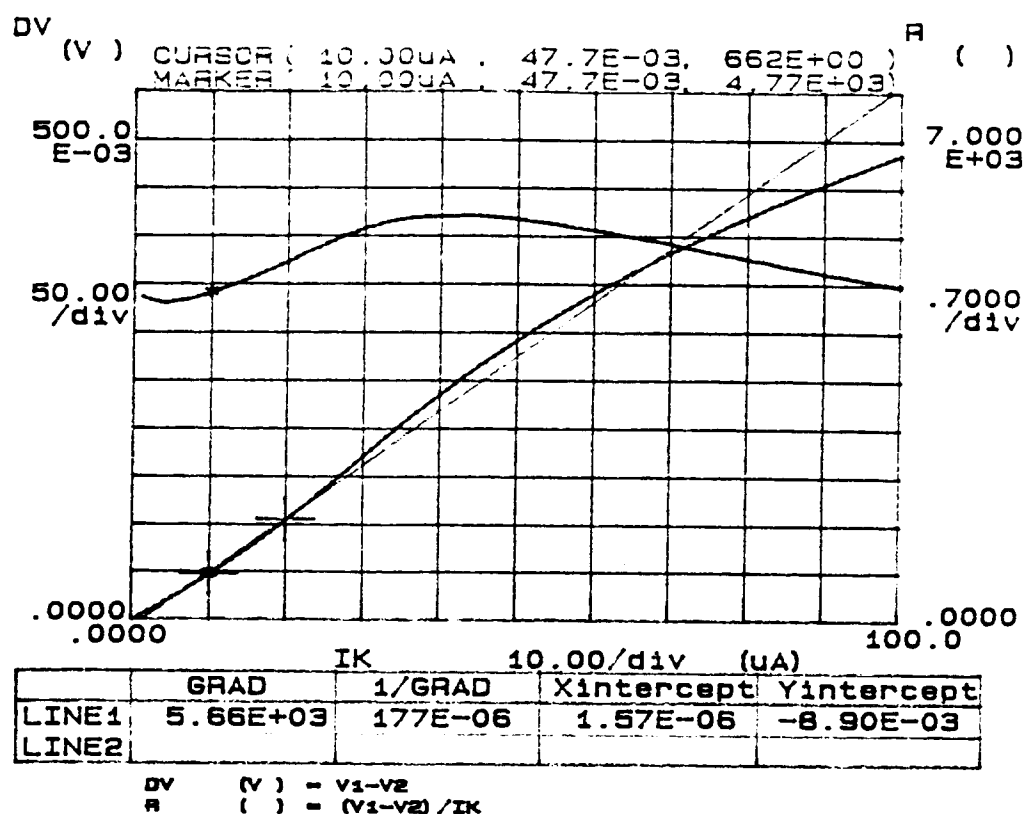


Fig. 15: I-V and resistance plot of a 50% over-etched RIE + EKC265 cleaned contact.

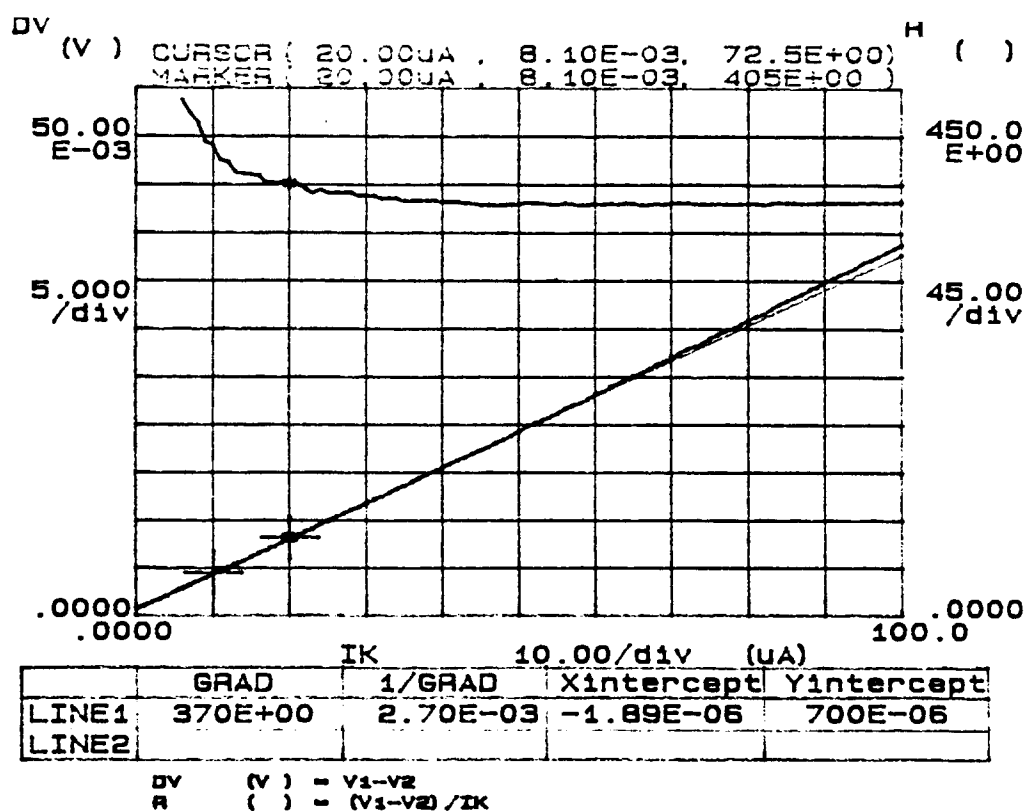


Fig. 16: I-V and resistance plot of a 50% over-etched RIE + O₂ annealed contact.

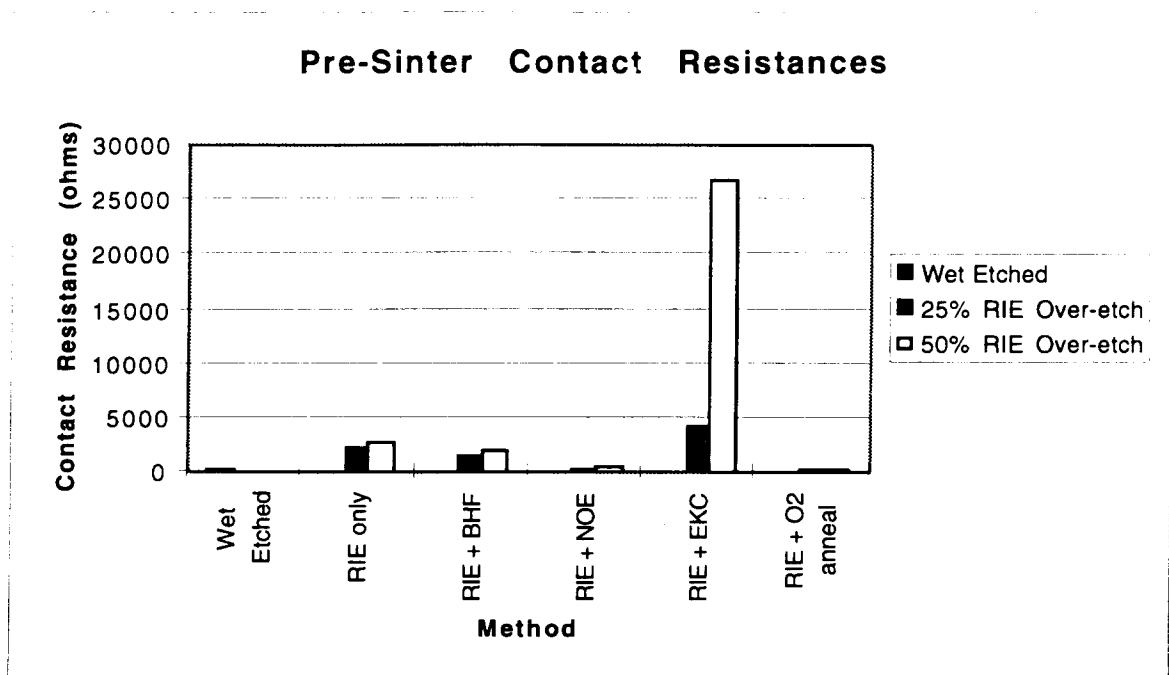


Fig. 17: Summary of the pre-sinter contact resistances of all the different methods evaluated.

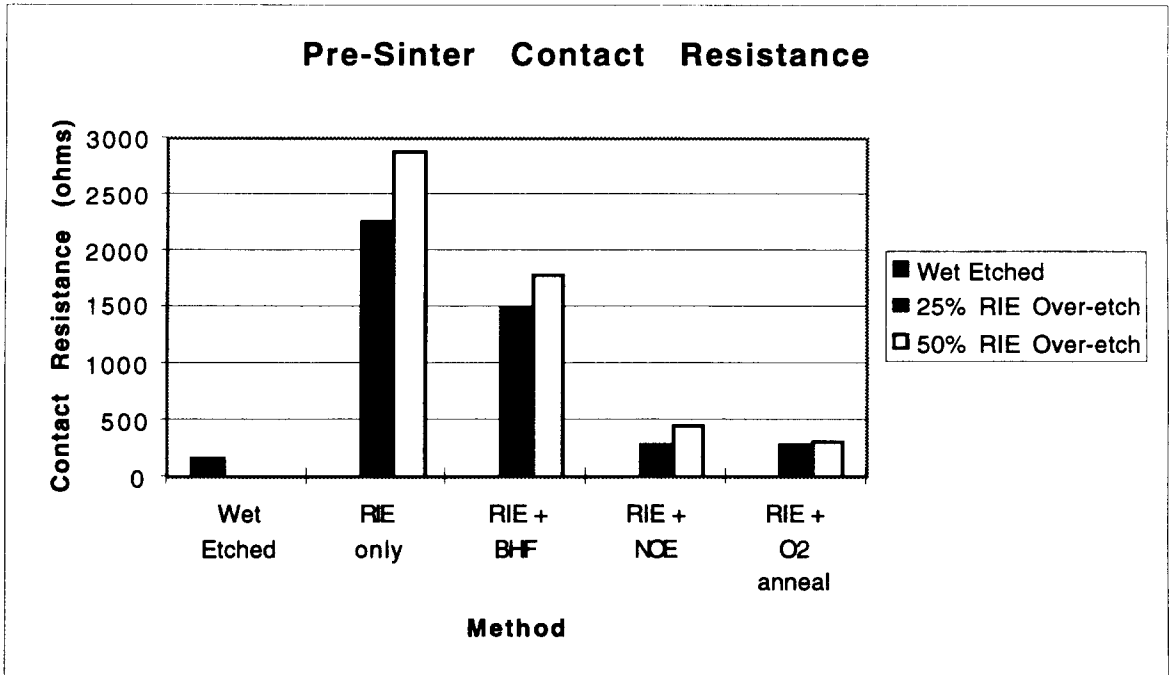


Fig. 18: Summary of the pre-sinter contact resistances of all the different methods evaluated, less the EKC265 method.

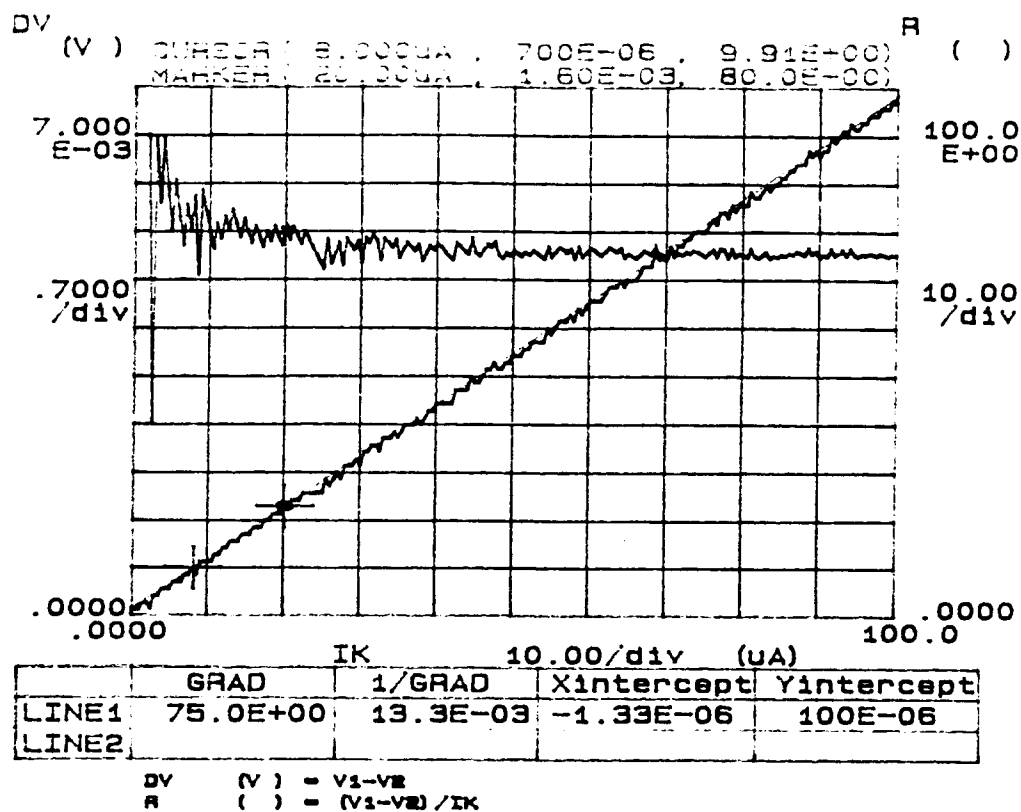


Fig. 19: I-V and resistance plot of a 50% over-etched RIE-only contact after sintering.

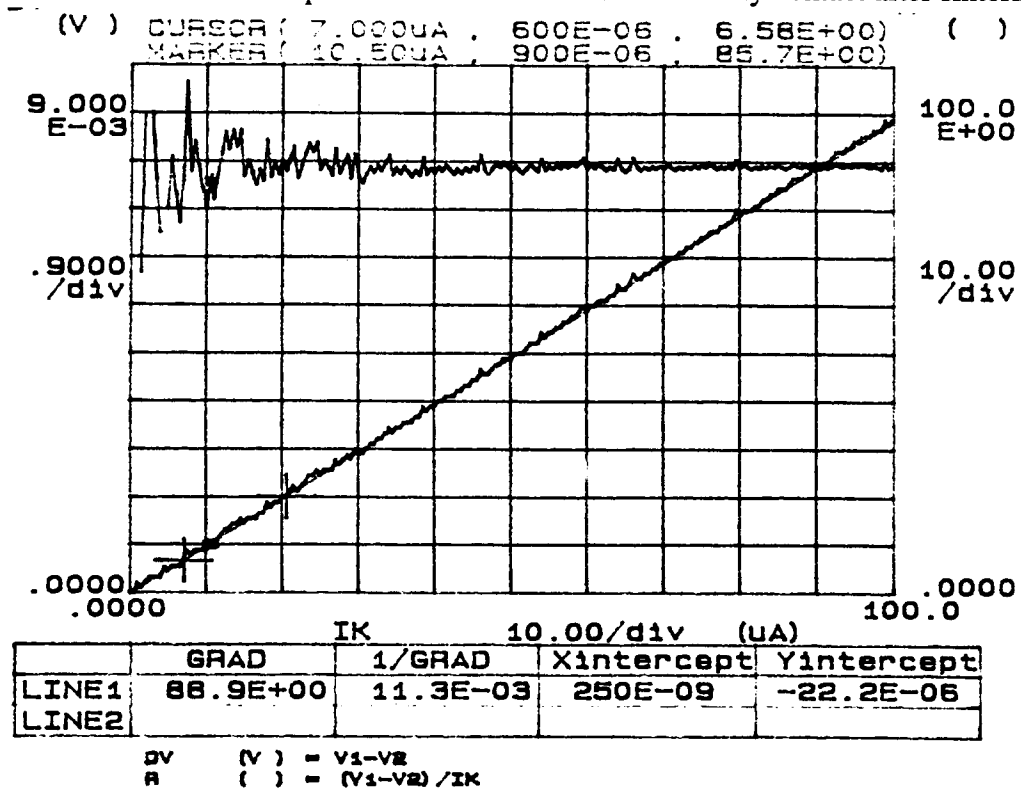


Fig. 20: I-V and resistance plot of a 50% over-etched RIE + BHF-dipped contact after sintering.

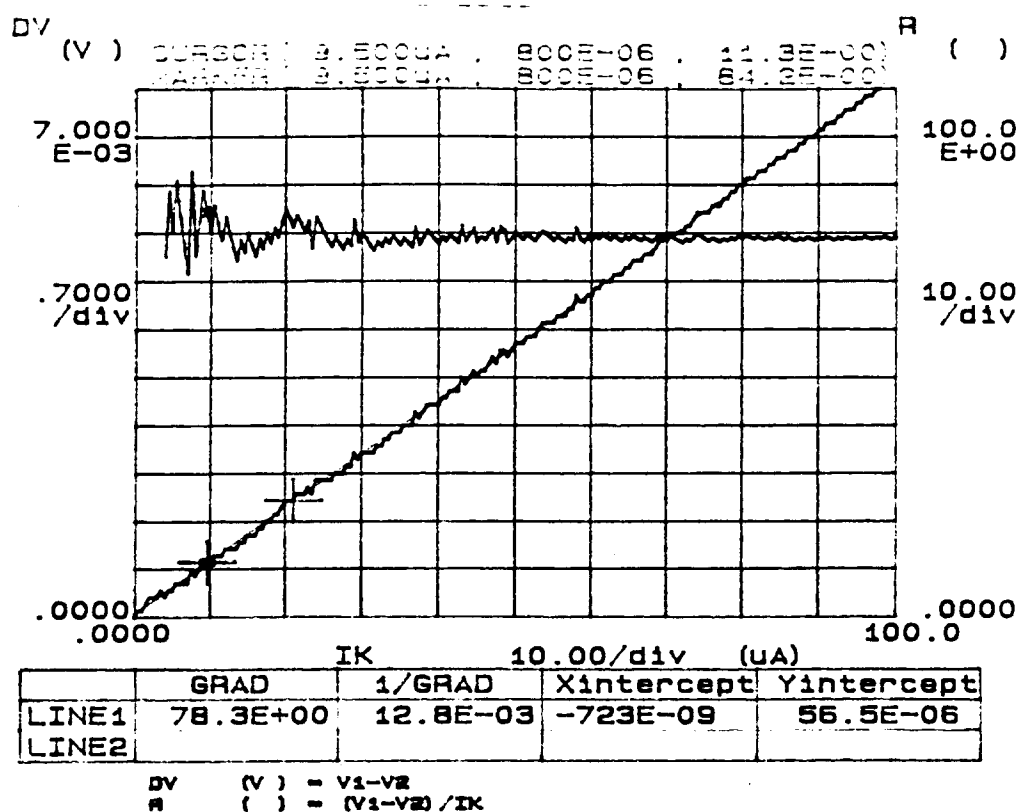


Fig. 21: I-V and resistance plot of a 50% over-etched RIE + NOE-cleaned contact after sintering.

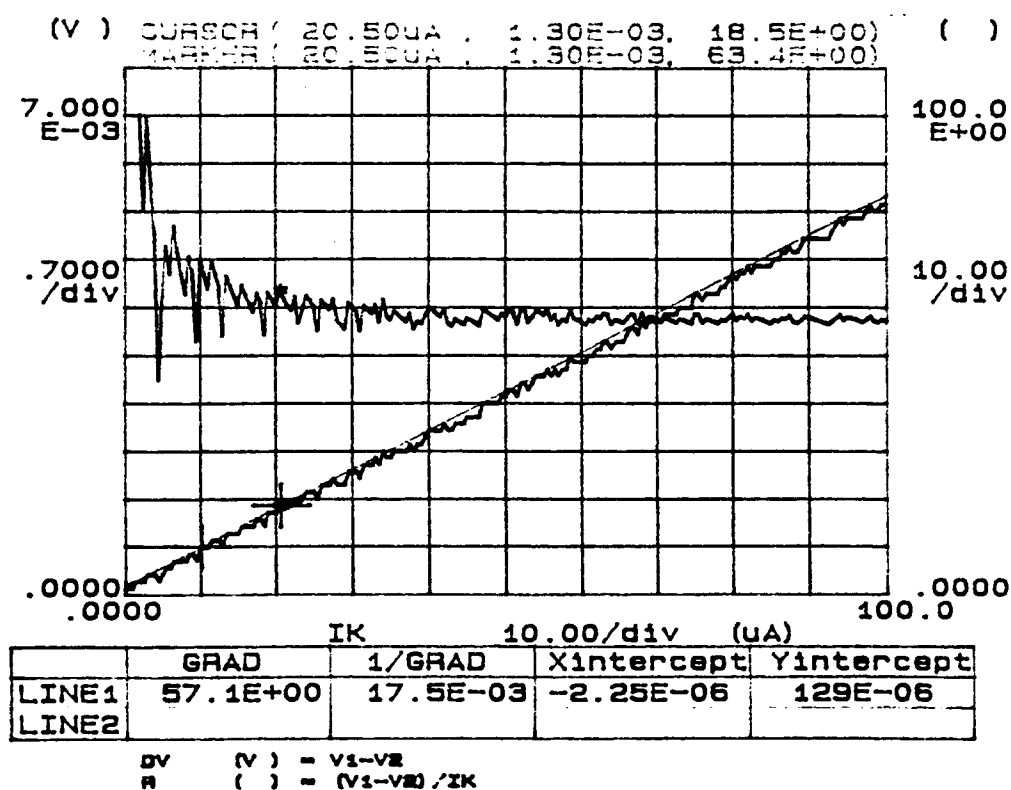


Fig. 22: I-V and resistance plot of a 50% over-etched RIE + EKC265-cleaned contact after sintering.

Post-Sinter Contact Resistance

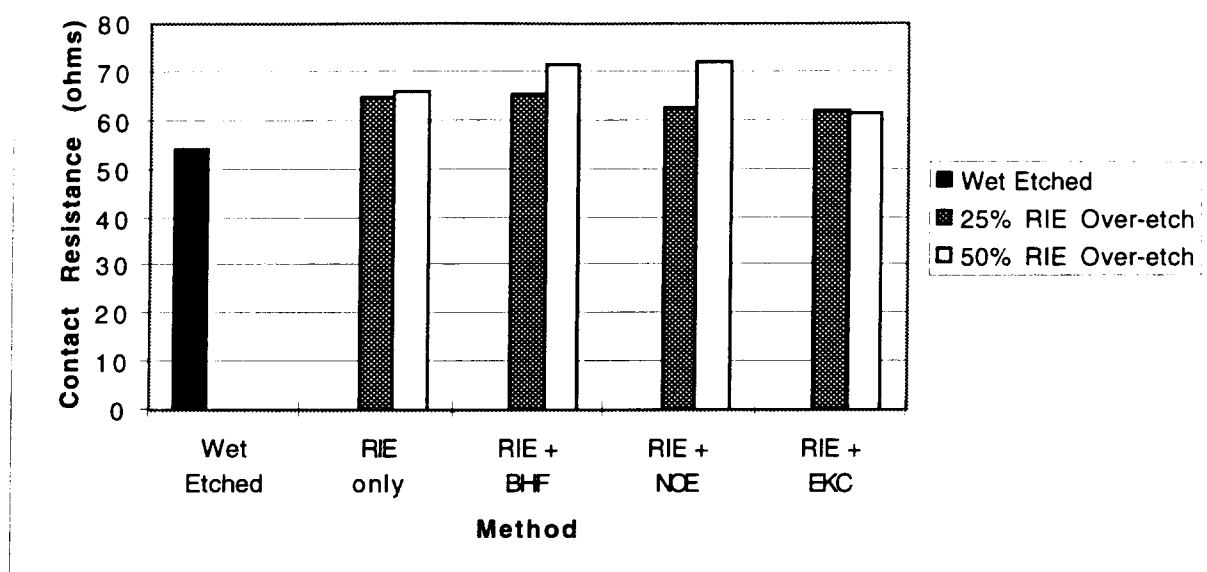


Fig. 23: Summary of the post-sinter contact resistances of all the different methods evaluated, less the O₂ anneal method.

Although the post-sintered measurements make it look like all of the techniques form suitable contacts, the contact resistances are still rather high and we are obviously having circuit problems using some of these approaches. The pre-sintered results in this sense are somewhat more telling. One problem may be in the method we are using for these measurements. By forcing a current through the contact at the 100 μ A level, a thin surface film may tend to break down, masking much of the film resistance. In the source or drain regions of a circuit MOSFET, a similar effect may occur, making the measurements relevant; however, gate contacts have no way to conduct dc current and such a film would never break down. In this sense the presence of a barrier film would not be seen but would still cause problems.

In order to further explore contact formation, we have also checked series-connected strings of 100 3 μ m \times 3 μ m contacts. These gave results similar to the pre-sintered results shown above, even after sintering. The reason may be that here there are 100 contacts and 100 surface films (if they exist) in series. Any applied voltage will be divided over all of them, and thus the series connection may not tend to break down as easily as the single Kelvin-bridge connection. Thus, the use of an RIE etch with an NOE descum or oxygen plasma would appear to be the best approach of all those tested to date. However, these still give contact resistances that are higher than desired. During the coming quarter, we will continue these studies. In addition, we will explore the use of sintered PtSi in the contacts and the use of TiN or TiW plugs. All of these techniques have been used extensively in the formation of integrated circuits over the coming decade. We also plan to complete the fabrication of a new round of active stimulating probes using the improved contact processes and apply them in demonstration studies in the guinea pig auditory system.

4. External Probe Interface Development

The goals for the next-generation of external interface systems are threefold: to increase the maximum bit rate of communication with the stimulating probe to 10MHz, to allow for greater flexibility in the bit-level communication protocol, and to reduce the complexity and cost of the system. Greater flexibility in the probe communication protocol will allow the interface system to be compatible with virtually any probe design. The reduced system complexity and cost will speed the development process and make the system more affordable, both for internal and external users.

The first design option considered was a simple upgrade of the current system, which has a maximum bit rate of 4MHz and is only able to interface with the STIM-1 and STIM-2 generation of probes. The current system consists of three hardware components: a Chimera PC plug-in board, a custom daughter board that attaches to the Chimera, and a custom remote converter board that drives the probe. The goals of a higher bit rate and flexible communication protocol were judged to be unattainable without a new hardware development effort that would essentially redesign both the daughter board and the remote converter. Given that a new hardware development effort is required, it is worthwhile to consider a different system architecture that can perhaps satisfy all of the design goals described above.

In the shorter term, a flexible communication protocol can be achieved by removing the current daughter board and replacing it with a simple pass-through system that directly connects the Chimera board with the remote converter. This places the communication protocol under control of the programmable Chimera processor, allowing for complete flexibility. It is impossible, however, to maintain a 10MHz bit rate with this arrangement, due to the real-time requirements placed on the Chimera processor and to the limitations of the physical connection between the Chimera and the remote converter. For immediate needs, however, a wire-wrap pass-through board can be constructed with relatively little effort that will allow the external system to drive a new probe design (incompatible with the STIM-1 or STIM-2 protocol). The maximum bit rate will be limited so that this system will only be useful for testing and low-speed applications. Existing software will have to be modified to support this new architecture.

In the long term, an alternative design is proposed that requires a new hardware development effort. This design, however, reduces the number of boards in the system from three to one single custom board while still meeting all of the design goals. A diagram of the system architecture is shown below in Fig. 24. This design was chosen after a review of existing DSP and controller boards available as PC plug-in boards. Systems that could sustain a high bit rate protocol were expensive and over-designed for this application. Simpler and less costly systems were flexible enough to implement an arbitrary communication protocol, but not at the high speeds required. In all cases, an extra custom hardware component was considered necessary for implementing the unique tri-level voltage connection to the stimulating probe. A fully custom design will require the same hardware development effort, but will not require an extra DSP or controller board.

The two key components of the proposed design are a microcontroller, for coordinating system functions, and a memory-driven microsequencer for implementing the bit level protocol. The use of memory to drive the sequencer allows for great flexibility in the protocol. The sequencer can be implemented in just a few components, yet will be able to sustain bit rates in excess of 10MHz. The microcontroller will have an integrated serial

port, dedicated I/O pins, and programmable timers, providing many of the basic system functions in a single device. This will keep the cost and the total part count low.

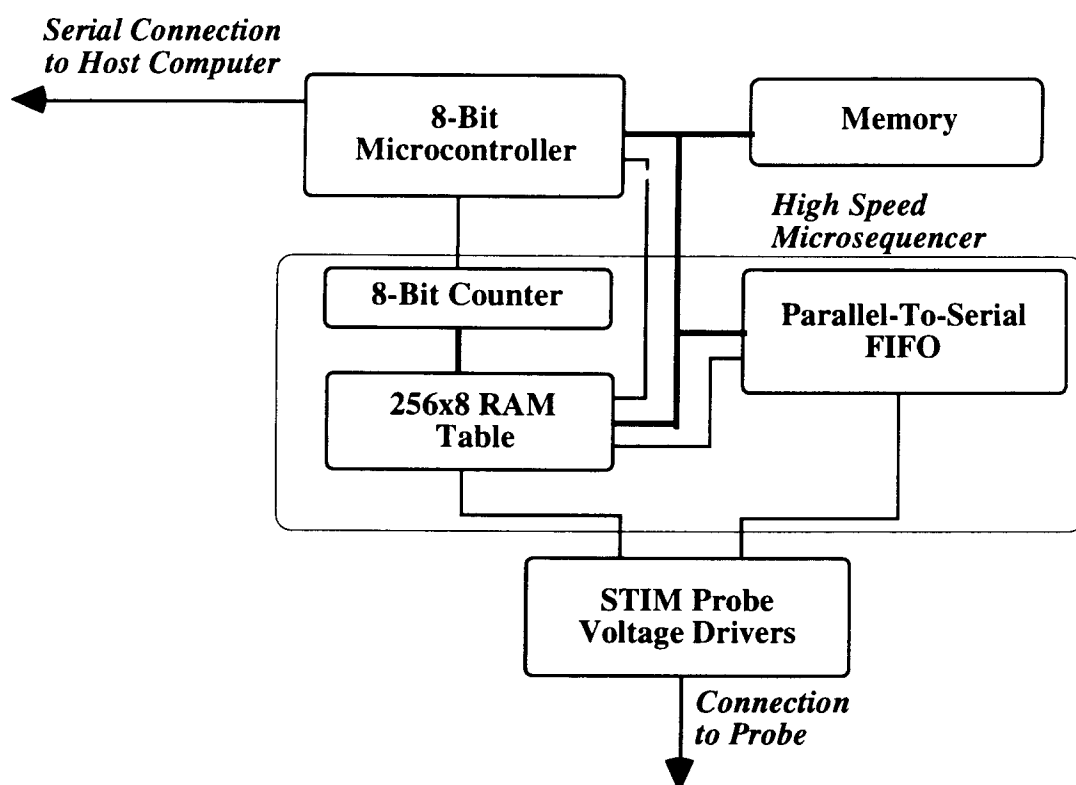


Fig. 24: Block diagram of a new interface being developed for the active stimulating probes.

This system would be completely self-contained and external to the host system. A standard serial interface to the host allows the use of any popular computer system with a serial port, such as an IBM PC compatible, a Macintosh, or a workstation-class machine to serve as the host. During the coming quarter, the design of both the temporary pass-through daughter board replacement and the new stand-alone system will proceed in parallel, with the balance determined by the needs of the greater project.

5. Conclusions

During the past quarter, work in this program has gone forward in several areas. We have continued to fabricate passive probe structures for internal and external users. Working in conjunction with the Center for Neural Communication Technology, additional probes from one mask set have been realized, a new mask set containing probe designs

from five external users has been designed, and probes from this new mask set are now in fabrication. We have also performed detailed characterization studies on chronically-implanted iridium oxide stimulating sites in-vivo. Electrochemical impedance spectroscopy (EIS) and cyclic voltammetry (CV) were used to evaluate chronically stimulated sites in six animal experiments in guinea pig cortex using 21 separate sites. The probes consisted of sites varying from $400\mu\text{m}^2$ to $1600\mu\text{m}^2$ in size. Stimulation began after a 10-17 day recovery period. Biphasic current pulses (variable magnitude, $100\mu\text{sec/phase}$, 250pps) were applied both bipolarly and monopolarly for two hours on five consecutive days. These current pulses reduced the charge storage and increased the site impedances at low frequencies, implying a change in the iridium oxide. The low-frequency change is permanent, in that a night of rest did not return the impedance spectrum to its pre-stimulation levels. Current pulsing also affects the impedance spectrum at mid-range frequencies, with the magnitude decreasing after stimulation. However, this decrease appears to be temporary, with magnitude returning to a higher value by the next day. The impedance change effected by current pulses takes place after a relatively few number of pulses have been applied. Additionally, some data suggests that a significant effect is seen in the electrical characteristics as a result of implantation. During the coming quarter, the data will be examined more analytically and the effects of encapsulation and healing will be examined more thoroughly. Histological results should also be available then for these experiments.

Two key areas in the further development of active stimulating probes involve the development of low-resistance interconnect materials and improvements in making circuit contacts. Both of these areas were undertaken during the past term. Both tantalum and titanium silicide interconnects were formed using co-sputtering and found to exhibit sheet resistances of about 3.5 ohms per square. This is three to four times better than the highly doped polysilicon currently used on the probes. We plan further experiments using refractory salicides, refractory metal cores, and optimization of the present co-sputtering approach to try to reduce the resistance another factor of three. In the area of circuit contacts, five different approaches to contact formation were explored in connection with the basic reactive ion etching process. Of these, the use of a modest RIE overetch followed by either an NOE descum cleaning step or an oxygen plasma cleaning step produced the best results. The contacts were greatly improved over other approaches, at least before sintering; after sintering all of the approaches appeared to produce similar results. Additional experiments to try to lower the contact resistances further are planned along with experiments using PtSi and TiN or TiW plugs in the contacts. Processing will then go forward to completion on a new set of active stimulating probes. The design of a new 64-site four-channel stimulating probe with off-chip current generation is also nearing completion.